

# THE MID-INFRARED SPECTRAL ENERGY DISTRIBUTION, SURFACE BRIGHTNESS AND COLOR PROFILES IN ELLIPTICAL GALAXIES

PASQUALE TEMI<sup>1,2</sup>, FABRIZIO BRIGHENTI<sup>3,4</sup>, WILLIAM G. MATHEWS<sup>3</sup>

*Draft version February 1, 2008*

## ABSTRACT

We combine 2MASS data and *Spitzer* archival data to study the emission in mid-infrared passbands (1.2 - 24 $\mu$ m) from a sample of 18 elliptical galaxies. In general the surface brightness distributions resemble de Vaucouleurs profiles, indicating that most of the emission arises from the photospheres or circumstellar regions of red giant stars. The spectral energy distribution peaks near the *H* band at 1.6 $\mu$ m. The half-light or effective radius has a pronounced minimum near the *K* band (2.15 $\mu$ m) with a second, less consistent minimum in the 24 $\mu$ m passband. All sample-averaged radial color profiles  $\langle \lambda_i - \lambda_j \rangle$  where  $\lambda_i < \lambda_j$  (and  $j \neq 24\mu$ m) have positive slopes within about twice the (*K* band) effective radius. Evidently this variation arises because of an increase in stellar metallicity toward the galactic cores. Color profiles  $\langle K - j \rangle$  all have positive slopes, particularly when  $j = 5.8\mu$ m although no obvious absorption feature is observed in spectra of elliptical galaxies near 5.8 $\mu$ m. This, and the minimum in  $R_e$ , suggests that the *K* band may be anomalously luminous in metal-rich stars in galaxy cores. Unusual radial color profiles involving the 24 $\mu$ m passband may suggest that some 24 $\mu$ m emission comes from interstellar not circumstellar dust grains.

*Subject headings:* galaxies: elliptical and lenticular; galaxies: ISM; infrared: galaxies; infrared: ISM

## 1. INTRODUCTION

Our curiosity about the mid-IR properties of elliptical galaxies arose from two motivations: the implications for stellar mass and light distributions and the transition from circumstellar dust to interstellar dust. Regarding the structure of elliptical galaxies, we were surprised that the effective (or half-light) radius  $R_e$ , a fundamental structural property of elliptical galaxies, was a surprisingly strong function of wavelength. Between the *V* and *K* bands the effective radius  $R_e$  decreases by more than 30 percent (Ko & Im 2005), reducing the “tilt” of the fundamental plane for elliptical galaxies from that expected for virialized homologous galaxies (e.g. Prugniel & Simien 1996). Radial variations in the mean stellar color can arise from variations in either stellar metallicity or age. However, it is generally accepted that the observed color variations in elliptical galaxies are due largely to metallicity (e.g. Sanchez-Blaquez et al. 2007). Photometric colors are affected by an increase in the spectral density and strengths of absorption lines (line blanketing) toward the galactic centers where the stellar metal abundance reaches its maximum value. When imaged in the light of optical photometric bands, line blanketing reduces the stellar emissivity and surface brightness in the galactic cores, resulting in an overall increase in the half-light radius when compared to the surface brightness profiles in relatively line-free near-IR photometric bands such as the *K* filter near 2 $\mu$ m. If the *K* band is essentially free of strong absorption and emission

features, as commonly supposed, we wondered if the effective radius would continue to decrease at wavelengths greater than the *K* band. More importantly, does the *K* band emission, or the emission from any other infrared band, accurately trace the stellar luminosity and mass in elliptical galaxies, or is it necessary to make bolometric corrections using the full spectral energy distribution at each radius?

Our second motivation to study the mid-IR color profiles in elliptical galaxies was to learn more about the transition of infrared-emitting dust from circumstellar to interstellar environments. In a recent paper we showed that the total luminosity of elliptical galaxies in *Spitzer*’s 24 $\mu$ m photometric band correlated with optical luminosity while luminosities at 60 and 170 $\mu$ m did not (Temi, Brighenti, & Mathews 2007). As dusty gas flows away from mass-losing red giant stars, it receives progressively less illumination from the photosphere of the parent star and relatively more collective diffuse radiation from distant galactic stars. Truly interstellar dust is heated at comparable rates by absorption of diffuse starlight and by inelastic impacts of thermal electrons in the hot interstellar gas. Both types of heating increase toward the galactic cores where the stellar and interstellar gas densities are largest. Does the 24 $\mu$ m emission from relatively cold dust in ellipticals vary with galactic radius in a manner that reveals a transition to interstellar heating patterns?

We describe below the surface photometry of a sample of elliptical galaxies in the *Spitzer* photometric passbands at 3.6, 4.5, 5.8, 8.0 and 24 $\mu$ m and compare them with similar 2MASS data at 1.2, 1.6 and the *K* band at 2.15 $\mu$ m. In general we find significant radial variations in colors formed by pairs of infrared bandpasses, particularly when the *K* band is involved. The atomic, molecular or dust spectral features responsible for these variations are currently unknown, but we discuss several possibilities.

<sup>1</sup> Astrophysics Branch, NASA/Ames Research Center, MS 245-6, Moffett Field, CA 94035.

<sup>2</sup> SETI Institute, Mountain View, CA 94043; and Department of Physics and Astronomy, University of Western Ontario, London, ON N6A 3K7, Canada. ptemi@mail.arc.nasa.gov

<sup>3</sup> University of California Observatories/Lick Observatory, Board of Studies in Astronomy and Astrophysics, University of California, Santa Cruz, CA 95064 mathews@ucolick.org

<sup>4</sup> Dipartimento di Astronomia, Università di Bologna, via Ranzani 1, Bologna 40127, Italy fabrizio.brighenti@unibo.it

Typical spectra of elliptical galaxies taken with the *Spitzer* Infrared Spectrograph (IRS) (Bregman, Temi & Bregman 2006; Bressan et al. 2007) have slope changes at about  $8\mu\text{m}$  which may mark the transition from photospheric emission to emission from circumstellar dust, probably silicates (Bressan et al. 2007), but this transition is unlikely to be abrupt. In any case, photospheric gas emission and circumstellar dust emission must be regarded as equally viable measures of stellar light in elliptical galaxies. It has been known for many years that the surface brightness profiles in these galaxies at  $10\text{--}12\mu\text{m}$  follows a de Vaucouleurs law similar to that of the optical light (Knapp, Gunn & Wynn-Williams 1992).

## 2. THE SAMPLE

We selected 18 elliptical galaxies from the *Spitzer* archives, emphasizing those with E classifications rather than E/S0 or S0. An attempt was made to select normal galaxies free of unusual masses of accreted cold gas, recent mergers or other such anomalies. We restricted the absolute magnitude to  $M_B > -18$  to avoid dwarf ellipticals. Most sample galaxies had been photometrically observed in the  $K$  band by Pahre (1999) and all but six were photometrically analyzed in the near-IR 2MASS survey (Jarrett 2003). As described below we photometrically extracted the  $K$  band surface brightness distributions and other photometric data directly from the 2MASS images for all galaxies in our sample including by necessity the six with unpublished 2MASS data. All sample galaxies were chosen so that the  $K$  band effective radius exceeds  $13''$ , allowing observations to extend well beyond the point response function at all infrared wavelengths. Our sample galaxies are listed in Table 1.

## 3. OBSERVATIONS

The data presented here were obtained with the Infrared Array Camera (IRAC) (Fazio et al. 2004) and the Multiband Imager Photometer (MIPS) (Rieke et al. 2004) on board the *Spitzer* Space Telescope (Werner et al. 2004). At all wavelengths full coverage imaging was obtained for all observations with additional sky coverage to properly evaluate the background emission. We used the Basic Calibrated Data (BCD) products from the Spitzer Science pipeline (version 14.0) to construct mosaic images for all objects. Pipeline reduction and post-BCD processing using the MOPEX software package (Makovoz et al. 2006) provide all necessary steps to process individual frames: dark subtraction, flat-fielding, mux-bleed correction, flux calibration, correction of focal plane geometrical distortion, and cosmic ray rejection.

Foreground stars and background galaxies were present in the final mosaiced images at all bands. These were identified by eye and cross-checked using surveys at other wavelengths (Digital Sky Survey and 2MASS). They were then masked out from each IRAC and MIPS image before isophotal fitting procedure was performed. Sky subtraction was performed by averaging values from multiple apertures placed around the target, avoiding any overlap with the faint extended emission from the galaxy.

When data are presented in the IRAC and MIPS magnitude system relative to Vega, we used the zero-magnitude flux densities presented in the instrument's manuals and published by Reach et al. (2005). Corrections for extended emission were also applied to the flux

densities as described in the Spitzer Observer's Manual. The uncertainties on the final absolute calibration are estimated at few percent at all 4 IRAC bandpasses and 10% for the  $24\mu\text{m}$  data.

## 4. SURFACE BRIGHTNESS PROFILES

Following a procedure similar to that used in the 2MASS survey (Jarrett 2003), our surface photometry is based on fitting elliptical apertures to galactic images in every infrared passband. This was accomplished using the ELLIPSE task in the ISOPHOTE package of IRAF. Bad pixels, superimposed stars and background objects were removed. We continue to the sky noise limit at which the mean brightness on the best-fitting ellipse is  $19\text{--}20\text{ mag arcsec}^{-2}$  in all passbands except at  $24\mu\text{m}$  where the sky cutoff is at  $17\text{--}18\text{ mag arcsec}^{-2}$ .

Figure 1 (top panel) shows the surface photometry for NGC 4472, a typical bright elliptical in our sample, plotted against  $R''^{1/4}$  where  $R$  is the radius of the local semimajor axis. For comparison we also show the surface brightness profile  $\mu_K(R)$  of an image in the 2MASS  $K_s$  filter. The bandpass of the 2MASS  $K_s$  filter ( $2.0 - 2.32\mu\text{m}$ ) differs slightly from the traditional Johnson  $K$  filter ( $2.03 - 2.42\mu\text{m}$ ; see Pahre 1999 for further details). For simplicity in the subsequent discussion we refer to the  $K_s$  filter simply as  $K$ . The surface brightness profiles  $\mu_i(R)$  at the IRAC photometric bands  $i = 3.6, 4.5, 5.8$  and  $8\mu\text{m}$  shown in Figure 1 overlap but are bounded below by  $\mu_K$  (solid line) and above by  $\mu_{24}$  (dotted line). While a de Vaucouleurs  $R^{-1/4}$  model is a good fit for all mid-IR wavelengths, small radial color variations between  $\mu_i(R)$  do occur and these are discussed below. Our full set of surface brightness data is available in electronic form at the ApJ website.

The lower two panels in Figure 1 show the spectral energy distributions (SED) for NGC 4472 in magnitude  $\text{arcsec}^{-2}$  and in  $\text{mJy arcsec}^{-2}$  plotted between the J ( $1.2\mu\text{m}$ ) and  $24\mu\text{m}$  MIPS bands. Small radial variations in the infrared SED are visible. The mean E galaxy infrared SED for all galaxies in our sample (arbitrarily normalized to the  $K$  band) is shown in Figure 2. Evidently the energy output of elliptical galaxies peaks near the  $H$  band ( $1.6\mu\text{m}$ ), in good agreement with the theoretical expectations (e.g. Piovan et al. 2003). Note that the sample-averaged  $\mu_{24}$  is enhanced toward the galactic center relative to other infrared passbands (also see Figs. 6 and 7 below). Although this  $24\mu\text{m}$  enhancement is less pronounced in NGC 4472 (Fig. 1), it is a general property of our sample galaxies.

Two galaxies in our sample – NGC 4697 and NGC 5322 – have atypical SEDs in the central  $\sim 5$  arcseconds. The first of these ellipticals has an unusually massive central dusty disk which, according to Bregman, Bregman, and Temi (2006) contains strong PAH emission possibly associated with a starburst that may have occurred some time ago. A small central dust lane in NGC 5322 has been described by Carollo et al. (1997). Infrared emission from these two central dust clouds is confined to the nucleus and does not contribute significantly to the color profiles discussed below which begin at  $\sim 6$  arcseconds.

## 5. EFFECTIVE RADIUS

The total magnitude of each galaxy at each infrared wavelength  $i$  can be found by integrating the surface

brightness  $\mu_i$  over area. This has been done in a sky-corrected manner by extending the observed  $\mu_i(R)$  with extrapolations to  $6R_e(K)$  assuming de Vaucouleurs profiles and uniform ellipticity in the extrapolated extensions. The effective or half-light radius  $R_e(i)$  at each infrared wavelength was then determined by integrating over the surface brightness to that radius  $R_e(i)$  enclosing half the total flux (data plus extrapolation). Since our photometric procedure is similar to that used in the 2MASS survey (Jarrett 2003), our values of  $R_e(K)$  determined from the 2MASS image should agree with 2MASS  $R_e(K)$  as tabulated by Jarrett and Figure 3 shows that this is indeed the case.

Figure 4 shows the ratio  $R_e(i)/R_e(K)$  for our sample galaxies plotted against  $R_e(K)$ . While there is some variation among the galaxies,  $R_e(i)$  is systematically larger than  $R_e(K)$  for all IRAC wavelengths except  $i = 24$  where the scatter is larger.  $R_e(J)$  and  $R_e(H)$  also tend to exceed  $R_e(K)$ , indicating a minimum half-light radius in the  $K$  band.

Figure 5 shows sample-averaged values of  $\langle R_e(i)/R_e(K) \rangle$  from  $i = V$  to 24 microns. The leftmost open diamond showing  $\langle R_e(V)/R_e(K) \rangle$  is based on  $R_e(V)$  for each sample galaxy taken from Faber et al. (1989), corrected slightly for seeing by Pahre (1999) using a program developed by Saglia et al. (1993). Circular aperture photometry is generally used in the Faber et al. compilation and a fully consistent ellipsoidal determination of  $R_e(V)$  would be slightly different. For comparison the + symbol shows  $\langle R_e(V)/R_e(K) \rangle = 1.33 \pm 0.40$  which is the mean ratio for all 273 early type galaxies in the Pahre (1999) sample (Ko & Im 2005). Finally, in computing  $\langle R_e(V)/R_e(K) \rangle$  for Figure 5 we excluded NGC 4696, the central and most luminous galaxy in the Centaurus Cluster. This galaxy has very extended stellar halo in the V band that must begin at a radius that exceeds the sky cutoff for all the IR bands. The infrared properties of NGC 4696 appear normal in other respects although this galaxy has an optically visible dust lane and is often classified as an S0.

Figure 5 clearly shows that the minimum effective radius occurs at the  $K$  band, although  $\langle R_e(24)/R_e(K) \rangle \approx 1$ . The steady decrease in the effective radius from the optical to the  $K$  band can be largely (or completely) explained by the decreasing influence of line blanketing toward the red. The unanticipated increase in  $R_e$  at 3.6 microns and beyond is likely to result from molecular and dust absorption as we discuss below.

Table 2 lists values of the effective radius  $R_e(i)$ , the surface brightness at the effective radius  $\mu_e(i) = \mu_i[R_e(i)]$ , and bandpass luminosities  $L_i$  for individual galaxies.

## 6. RADIAL COLOR GRADIENTS

Figures 6 and 7 show infrared color gradients  $\mu(i) - \mu(j)$  averaged over our sample galaxies. This is done in several steps. First the  $\mu(i) - \mu(j)$  profile for each galaxy is plotted against physical radius normalized to the effective radius  $R_e(K)$  for that galaxy. Then plots of  $\mu(i) - \mu(j)$  for all sample galaxies are binned in  $\Delta[R/R_e(K)]$  and averaged as shown in Figures 6 and 7. Consequently, the error bars in Figures 6 and 7 show the typical  $1\sigma$  dispersion of sample galaxies from the mean color profiles in each bin; they do not imply that the shapes of the pro-

files are uncertain by this amount since the profiles tend to be remarkably similar for most sample galaxies. Color profiles involving  $24\mu\text{m}$  were scaled downward for comparison with other profiles. We show in the Appendix that the point spread functions in the  $K$ , IRAC, and  $24\mu\text{m}$  passbands are small and do not substantially alter the surface brightness color variations in Figures 6 and 7.

In general we see that infrared colors are quite sensitive to radial stellar population variations in elliptical galaxies. In principle, color gradients can arise from radial variations of stellar metallicity or mean stellar age, but recent detailed radial-dependent population models show that metallicity is by far the dominant source of color gradients (Sanchez-Blaquez et al. 2007).

Assuming that metallicity is the primary driver for the radial color variations in Figures 6 and 7, we attempted to compare mean colors in our sample galaxies with global metal abundances determined from optical line indices. For example we plotted all the colors discussed above averaged at  $R_e(K)$ ,  $R_e(K)/2$  and  $R_e(K)/4$  against the metal abundances recently determined by Sanchez-Blaquez et al. (2006) who studied many of the galaxies in our sample. This resulted in scatter diagrams because the errors in the metal abundances of individual galaxies using optical line indices are comparable to the complete range of metal abundances in our sample. Since the stellar metal abundance is known to increase with total luminosity, we also sought correlations of color-related parameters with the luminosity of each sample galaxy but, as before, no correlation emerged.

## 7. DISCUSSION

Relatively little is understood about the detailed mid-IR spectra of metal (and oxygen) rich giant stars expected in elliptical galaxies; the most relevant observations may be the 5 -  $17\mu\text{m}$  spectra of Milky Way Bulge AGB stars (Blommaert et al. 2006). However, it is well known from studies of globular clusters that the red giant branch cools with increasing metallicity (e.g. Ferraro et al. 2000), allowing molecular formation. Consequently, it is likely that molecular or dust spectral features contribute to the mid-IR spectrum and to the color variations we observe.

The  $\langle K - 24 \rangle$  and  $\langle 4.5 - 24 \rangle$  color profiles in Figures 6 and 7 are quite peculiar so we begin by discussing the colors between other passbands. In particular we see in Figure 7 that colors formed among the 3.6, 4.5 and  $8.0\mu\text{m}$  bands have the smallest slopes. One might imagine therefore that these three bands are uniquely free of metal lines or other metal-dependent spectral features, but such a conclusion would probably be premature. Nevertheless it is remarkable that the colors in Figure 6 formed by combinations of these three passbands with the  $K$  band -  $\langle K - 3.6 \rangle$ ,  $\langle K - 4.5 \rangle$ , and  $\langle K - 8.0 \rangle$  - have much larger positive slopes than  $\langle 4.5 - 8 \rangle$  or  $\langle 3.6 - 4.5 \rangle$ , so the  $K$  band is sensitive to gradients in the stellar metal abundance. The sense of the positive slopes in Figures 6 for colors  $\langle K - i \rangle$  where  $\lambda_K < \lambda_i$  is either that the  $i$  band is more strongly absorbed in the high metallicity core or the  $K$  band has an emission feature there. Emission in the  $K = K_s$  band ( $2.0 - 2.32\mu\text{m}$ ) seems unlikely. The Brackett- $\gamma$  line ( $2.16\mu\text{m}$ ) is not expected to appear strongly in emission when the Balmer lines themselves

are weak or absent and the CO band heads longward of  $2.29\mu\text{m}$ , if present in emission, affect only a small part of the  $K_s$  band and are more likely to appear in absorption (e.g. Cunha & Smith 2006). The colors in Figure 6 with the greatest positive slopes,  $\langle K - 5.8 \rangle$  and  $\langle K - 8.0 \rangle$ , are interesting because the  $5.8\mu\text{m}$  ( $4.97 - 6.47\mu\text{m}$ ) and  $8.0\mu\text{m}$  ( $6.37 - 9.53\mu\text{m}$ ) bandpasses are visible in  $5\text{-}20\mu\text{m}$  IRS spectra taken with *Spitzer* (Bregman, Temi & Bregman 2006; Bressan et al. 2007). These spectra, which are in good agreement with IRAC photometry, show no visible systematic absorption near  $5.8$  or  $8.0\mu\text{m}$  that would be needed to account for the positive slopes of  $\langle K - 5.8 \rangle$  and  $\langle K - 8.0 \rangle$  in Figure 6. However, it is possible that some broad band dust absorption is present at all IRAC wavelengths in the circumstellar regions of metal rich stars. If so, some enhanced solid phase absorption near  $5.8\mu\text{m}$  would be needed to account for the larger slope of  $\langle K - 5.8 \rangle$ .

In view of these unsatisfactory and somewhat contradictory arguments, we are led to speculate that the  $K$  band may be largely free of intrinsic absorption (or emission) features in the metal rich cores of these galaxies but that considerable widely distributed line or dust absorption exists to the blue (and possibly also to the red) of the  $K$  band. Under these circumstances, radiation at wavelengths adjacent to the  $K$  band could be absorbed and reprocessed in the stellar atmospheres until it preferentially emerges in the  $K$  band, resulting in an anomalously enhanced emission there. This hypothesis is also consistent with Figure 5 in which the  $K$  band has the smallest effective radius, i.e. its radiation is most strongly peaked in the central, most metal-rich regions of the galactic cores. An alternative, less likely, possibility for an enhanced  $K$  band is emission from hot, newly formed dust grains having a restricted range of temperatures and emissivities that peak in the  $K$  band.

The strange non-monotonic color profiles for  $\langle K - 24 \rangle$  and  $\langle 4.5 - 24 \rangle$  in Figures 6 and 7 may be related to an additional interstellar component in the  $24\mu\text{m}$  emission. To explore the possibility that these cold grains are heated by diffuse starlight, we compared  $\langle K - 24 \rangle$  with the local mean intensity of galactic stars. Specifically, we evaluated  $\langle K - 24 \rangle$  near  $R = R_e(K)/2$  for each sample galaxy and compared this with  $J_B[R_e(K)/2]$ , the mean diffuse  $B$  band intensity at this same radius found by using (spherical) de Vaucouleurs profiles and distances from Table 1 (Temi, Brighenti & Mathews 2007). This comparison, shown in Figure 8, appears indecisive due to the large scatter. The two relatively low luminosity galaxies at the far right, NGC 584 and 3379, have larger  $J_B$  because of the stronger stellar concentration in low luminosity ellipticals. While NGC 584 is classified as an E4 in RC2, Sandage & Bedke (1994) argue that it is an S0. Many authors have claimed that NGC 3379 is a face-on S0 (Capaccioli et al. 1991; Statler & Smecker-Hane 1999; see Harris et al. 2007 for a recent discussion). NGC 584 is certainly a flat galaxy and if NGC 3379 is also a flat S0 galaxy viewed face-on, we may have overestimated  $J_B$  of both galaxies by assuming that they are spherically symmetric. If these two galaxies are removed (or shifted to the left), the positive correlation visible in Figure 8 would be strengthened and this would be consistent with (stochastic) emission from small grains at  $24\mu\text{m}$ . However, data from additional galaxies will be

needed to confirm this.

Finally, in the infrared SEDs predicted by Piovan et al. (2003) the  $\langle K - 24 \rangle$  colors are expected to be enhanced in younger galaxies or in galaxies with a subcomponent of younger stars. When  $\langle K - 24 \rangle$  for our sample galaxies are plotted against ages estimated from stellar indices, there is some hint of a negative correlation, but our sample is too small and the ages too uncertain to be confident.

## 8. CONCLUSIONS

Our study of the mid-IR photometric properties of 18 elliptical galaxies from  $1.2\mu\text{m}$  to  $24\mu\text{m}$  resulted in the following conclusions:

- (1) The surface brightness distributions at all photometric passbands between  $1.2$  and  $24\mu\text{m}$  show good agreement with de Vaucouleurs  $R^{-1/4}$  profiles. However, small deviations do exist among the passbands, resulting in significant radial color gradients.
- (2) The sample-averaged spectral energy distribution (SED) for elliptical galaxies peaks at  $\sim 1.6\mu\text{m}$  near the  $H$  band and exhibits a small variation with galactic radius. Emission at  $5.8$  and  $8\mu\text{m}$  is systematically slightly lower near the galactic cores but emission at  $24\mu\text{m}$  becomes stronger there.
- (3) The effective radius  $R_e$  varies among various infrared passbands and has a sharp minimum at  $2.15\mu\text{m}$  in the  $K$  band.  $R_e$  at  $24\mu\text{m}$  is also small but there is more variation among individual galaxies.
- (4) Except for colors involving the  $24\mu\text{m}$  passband, all radial sample-averaged color profiles  $\langle i - j \rangle$  where  $\lambda_i < \lambda_j$  have positive slopes within about  $2R_e(K)$ , suggesting a sensitivity to stellar metallicity which decreases with galactic radius. However, the slope variations of individual color profiles are somewhat enigmatic in detail. All color profiles involving the  $K$  band,  $\langle K - i \rangle$ , have pronounced positive slopes. For example the radial color profiles  $\langle 3.6 - 4.5 \rangle$  and  $\langle 4.5 - 8 \rangle$  are rather flat while  $\langle K - 3.6 \rangle$  and  $\langle K - 4.5 \rangle$  have significantly larger positive slopes. The variation of  $\langle K - 5.8 \rangle$  is comparable to that in  $B - I$ . These results may suggest an anomalously enhanced emission in the  $K$  band from metal rich stars, possibly detracting from the common use of  $K$  band emission as an abundance-independent measure of local stellar mass. Centrally enhanced  $K$  band emission is also consistent with the minimum effective radius in this passband.
- (5) The sample-averaged radial color variations for the various mid-IR passbands  $i$  are consistent with the ratios of the half-light radii. For example,  $\langle R_e(3.6)/R_e(4.5) \rangle$  is nearly unity and the mean radial color profile  $\langle 3.6 - 4.5 \rangle$  is flat with radius. By contrast,  $\langle R_e(5.8)/R_e(K) \rangle$  is large and the radial variation of  $\langle K - 5.8 \rangle$  has a correspondingly larger positive slope.
- (6) Colder grains that emit at longer wavelengths are generally more distant from their parent red giant star. Eventually, as grains move very far from the parent star, they are heated more by diffuse interstellar starlight or collisional impacts than by light from the parent star. Although the integrated emission in the  $24\mu\text{m}$  passband is mostly circumstellar (Temi, Brighenti & Mathews 2007), we find that radial color profiles formed with the  $24\mu\text{m}$  passband have uniquely peculiar shapes. For example, our sample-averaged  $\langle K - 24 \rangle$  color profile has a maximum near  $0.5R_e(K)$ . This may indicate a transition to

interstellar heating for the grains emitting at this long wavelength, but our sample is too small to verify this with confidence.

This work is based on observations made with the Spitzer Space Telescope, which is operated by the Jet Propulsion Laboratory, California Institute of Technol-

ogy, under NASA contract 1407. Support for this work was provided by NASA through Spitzer Guest Observer grant RSA 1276023. Studies of the evolution of hot gas in elliptical galaxies at UC Santa Cruz are supported by a Spitzer Theory Grant, NASA grants NAG 5-8409 & ATP02-0122-0079 and NSF grant AST-0098351 for which we are very grateful.

## REFERENCES

- Blommaert, J. A. D. L., et al. 2006, *A&A*, 460, 555  
 Bregman, J. D., Bregman, J. N. & Temi, P. 2006, (astro-ph/0604369)  
 Bregman, J. N., Temi, P. & Bregman, J. D. 2006, *ApJ*, 647, 265  
 Bressan, A., et al. 2007, (astro-ph/0701620)  
 Capaccioni, M., et al. 1991, *ApJ*, 371, 535  
 Carollo, C. M., Franx, M., Illingworth, G. D., & Forbes, D. A. 1997, *ApJ*, 481, 710  
 Cunha, K. & Smith, V. V., 2006, *ApJ*, 651, 491  
 Faber, S. M., Wegner, G., Burstein, D., Davies, R. L., Dressler, A., Lynden-Bell, D., & Terlevich, R. J. 1989, *ApJS*, 69, 763  
 Fazio, G. G. et al. 2004, *ApJS*, 154, 10  
 Ferraro, F. R., Montegriffo, P., Origlia, L. & Fusi Pecci, F. 2000, *AJ*, 119, 1282  
 Harris, W. E., et al. 2007, *ApJ*, 667, 000 (arXiv:0706.1995)  
 Jarrett, T. H. 2003, *AJ*, 125, 525  
 Knapp, G. R., Gunn, J. E. & Wynn-Williams, C. G., 1992, *ApJ*, 399, 76  
 Ko, J. & Im, M. 2005, *Jour. Korean Astron. Soc.*, 38, 135  
 Makovoz, D., Trey, R., Khan, I., & Booth, H. 2006, *SPIE*, 6274, 10  
 Pahre, M. A. 1999, *ApJS*, 124, 127  
 Piovan, L., Tantalò, R. & Chiosi, C. 2003, *A&A*, 393, 149  
 Prugniel, Ph. & Simien, F. 1996, *A&A*, 390, 749  
 Reach, T. W. et al. 2005, *PASP*, 117, 978  
 Rieke, G. H. 2004, *ApJS*, 154, 25  
 Saglia, R. P. et al., 1993, *MNRAS*, 264, 961  
 Sanchez-Blazquez, P., Forbes, D., Strader, J., Brodie, J. & Proctor, R. 2007, *MNRAS*, 377, 759  
 Sanchez-Blazquez, P., Gorgas, J., Cardiel, N., & Gonzalez, J. J., 2006, *A&A*, 457, 809  
 Sandage, A. & Bedke, J. 1994, *The Carnegie Atlas of Galaxies*, v. 1  
 Statler, T. S. & Smecker-Hane, T. 1999, *AJ*, 117, 839  
 Temi, P., Brighenti, F., & Mathews, W. G. 2007, *ApJ*, 660, 1215  
 Werner, M. W., et al. 2004, *ApJS*, 154, 1

TABLE 1  
BASIC PROPERTIES OF THE SAMPLE

NGC	Type	T <sup>a</sup>	$d^b$ (Mpc)	Log $L_B^b$ ( $L_{B,\odot}$ )	2MASS? <sup>c</sup>
584	E4	-4.6	23.76	10.42	yes
2300	Sa0	-3.4	29.65	10.47	yes
3377	E4-5	-4.8	10.71	9.78	yes
3379	E1	-4.8	10.71	10.12	yes
3923	E4-5	-4.6	19.10	10.58	yes
4365	E3	-4.8	17.06	10.40	yes
4406	E3	-4.7	17.06	10.72	yes
4472	E2/S0	-4.8	17.06	10.96	yes
4636	E/S0	-4.8	17.06	10.57	yes
4696	E+1	-3.7	39.65	10.99	yes
4697	E6	-4.8	16.22	10.61	yes
5044	E0	-4.7	32.36	10.76	no
5322	E3-4	-4.8	29.79	10.73	yes
5557	E1	-4.8	49.02	10.90	no
5813	E1-2	-4.8	40.67	10.70	yes
5831	E3	-4.8	24.55	10.09	no
5845	E	-4.8	24.55	9.62	no
5846	E0-1	-4.7	24.55	10.72	no
6703	SA0	-2.8	32.06	10.43	no

<sup>a</sup> The morphological type T is taken from the HyperLeda database. <sup>b</sup> Distances and Luminosities are calculated with  $H_0 = 70 \text{ km s}^{-1} \text{ Mpc}^{-1}$ . <sup>c</sup> Availability of photometric data at the 2MASS website.

TABLE 2  
MID-IR PHOTOMETRIC DATA

Effective Radius $R_e(i)$ ( $''$ )						
NGC	$K$	$3.6\mu\text{m}$	$4.5\mu\text{m}$	$5.8\mu\text{m}$	$8\mu\text{m}$	$24\mu\text{m}$
584	23.64	25.71	27.10	29.15	28.80	23.82
2300	22.78	22.02	21.62	23.93	22.66	25.34
3377	25.48	29.50	29.58	31.88	30.65	27.57
3379	29.82	35.06	34.06	34.56	36.30	22.87
3923	40.25	47.67	47.76	48.66	49.78	47.01
4365	37.78	44.22	44.20	47.38	47.85	41.67
4406	59.13	62.10	62.30	58.53	58.28	52.32
4472	55.86	64.73	63.92	59.48	67.88	51.79
4636	56.29	62.61	61.73	62.92	61.65	58.90
4696	40.51	46.53	47.88	48.46	50.05	49.99
4697	39.58	45.16	50.02	56.49	53.59	29.72
5044	...	49.88	48.78	48.87	50.16	43.17
5322	31.31	34.56	34.49	38.10	37.44	16.91
5557	...	24.07	25.58	25.44	24.07	15.15
5813	36.17	43.31	42.6	52.60	47.10	22.71
5831	19.43	20.67	21.03	23.77	23.76	...
5846	35.75	42.82	44.51	42.75	43.83	38.44
6703	20.11	20.16	20.28	25.65	19.74	20.64
Surface Brightness $\mu_e(i)$ at $R_e(i)$ ( $\text{mag } (')^{-2}$ )						
NGC	$K$	$3.6\mu\text{m}$	$4.5\mu\text{m}$	$5.8\mu\text{m}$	$8\mu\text{m}$	$24\mu\text{m}$
584	17.11	17.08	17.24	17.31	17.18	15.71
2300	17.54	17.34	17.38	17.52	17.37	16.26
3377	17.31	17.25	17.26	17.31	17.28	16.02
3379	16.93	16.99	17.00	16.95	16.98	14.93
3923	17.57	17.45	17.50	17.42	17.46	16.02
4365	17.64	17.69	17.76	17.73	17.71	16.53
4406	17.89	17.83	17.90	17.68	17.63	16.45
4472	17.26	17.29	17.35	17.15	17.32	15.57
4636	18.18	18.23	18.24	18.20	18.24	18.50
4696	18.03	18.03	18.15	18.08	18.12	16.60
4697	17.34	17.06	17.29	17.47	17.26	15.21
5044	...	18.70	18.74	18.25	18.23	16.98
5322	17.46	17.57	17.60	17.67	17.60	14.79
5557	...	17.73	17.90	17.52	17.40	15.58
5813	18.04	18.18	18.19	18.40	18.21	16.02
5831	17.82	17.88	17.95	18.14	18.04	...
5846	17.60	17.94	18.06	17.87	17.89	16.35
6703	17.85	17.72	17.76	18.04	17.58	16.09
Bandpass Luminosities $L(i)$ ( $\text{erg s}^{-1}$ )						
NGC	$K$	$3.6\mu\text{m}$	$4.5\mu\text{m}$	$5.8\mu\text{m}$	$8\mu\text{m}$	$24\mu\text{m}$
584	43.01	42.61	42.32	42.09	41.90	40.89
2300	43.07	42.69	42.40	42.15	41.94	40.88
3377	42.26	41.92	41.66	41.40	41.19	40.04
3379	42.73	42.37	42.09	41.83	41.63	40.40
3923	43.14	42.79	42.51	42.30	42.07	40.87
4365	42.99	42.62	42.34	42.11	41.92	40.60
4406	43.20	42.82	42.54	42.27	42.07	40.86
4472	43.48	43.12	42.83	42.55	42.40	41.13
4636	43.07	42.70	42.41	42.17	41.96	40.67
4696	43.52	43.18	42.91	42.66	42.48	41.26
4697	43.05	42.70	42.45	42.23	42.05	40.68
5044	...	42.97	42.67	42.54	42.38	41.02
5322	43.26	42.90	42.63	42.40	42.22	41.10
5557	...	43.08	42.80	42.64	42.43	41.08
5813	43.19	42.86	42.57	42.39	42.14	40.77
5831	...	42.33	42.05	41.80	41.61	...
5846	43.18	42.88	42.61	42.36	42.16	40.99
6703	...	42.63	42.36	42.15	41.88	40.88

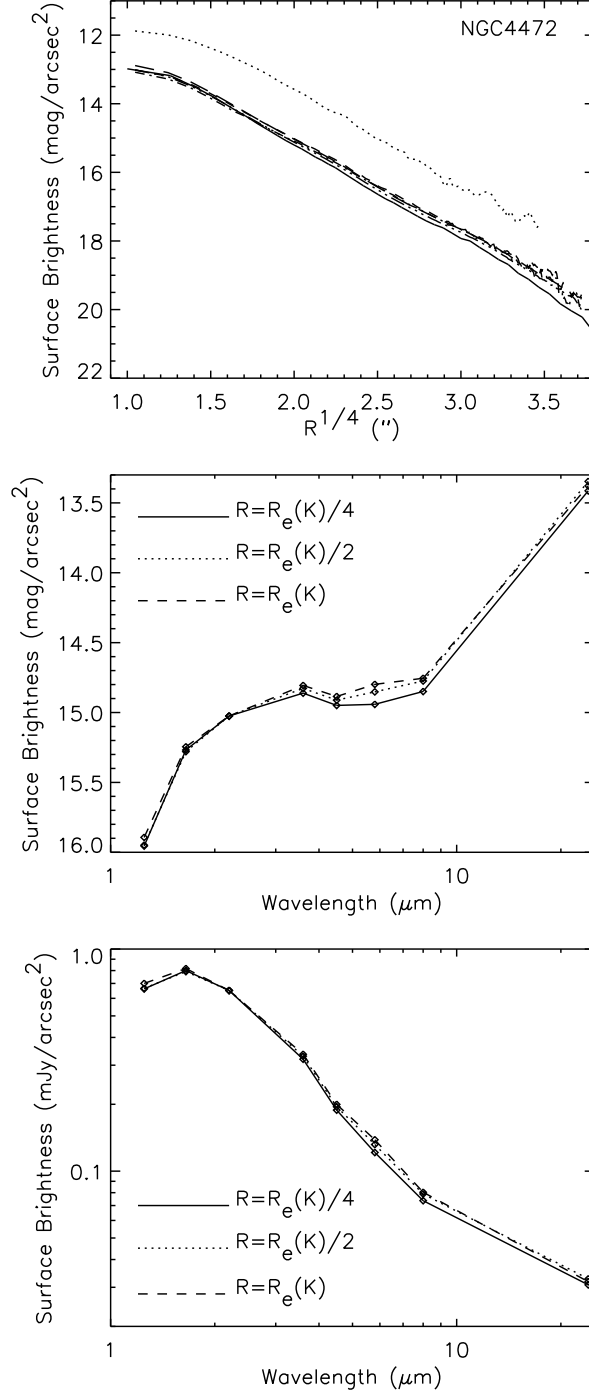


FIG. 1.— Mid-infrared surface brightness and spectral energy distributions (SEDs) for NGC 4472. *Top panel:* surface brightness profiles at six mid-infrared passbands:  $K$  band (solid line), IRAC 3.6, 4.5, 5.8 and  $8.0\mu\text{m}$  bands (having different line types but strongly overlapping), and MIPS  $24\mu\text{m}$  (dotted line). *Central panel:* Spectral energy distributions  $\mu_i$  and evaluated at three different radii in units of magnitude  $\text{arcsec}^{-2}$ . The data points refer from left to right to the  $i = J, H, K, 3.6, 4.5, 5.8, 8.0$  and  $24\mu\text{m}$  passbands. The SEDs are arbitrarily normalized to the  $K$  band. *Bottom panel:* Identical to the central panel except the surface brightness is given in  $\text{mJy arcsecond}^{-2}$ .

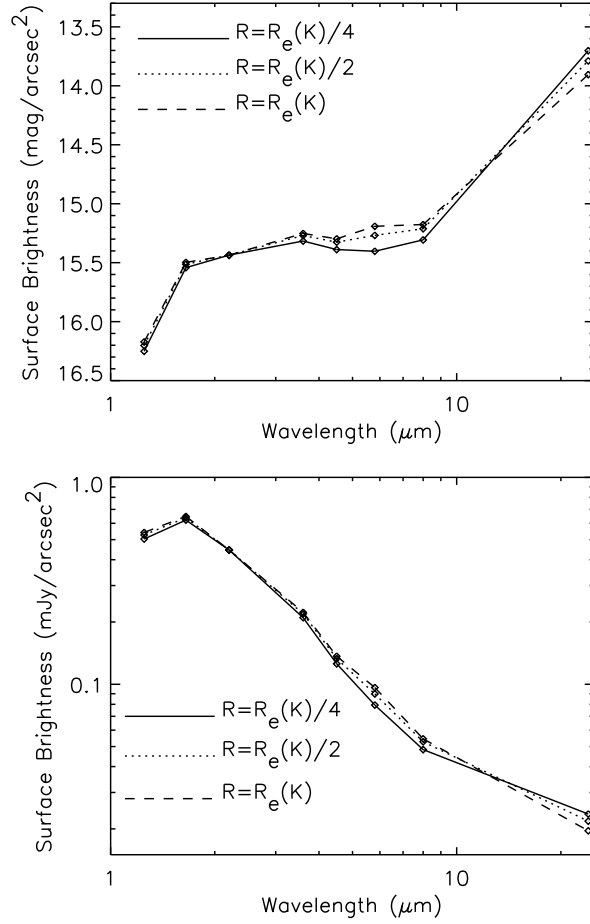


FIG. 2.— Sample-averaged SEDs at three radii normalized with  $R_e(K)$  and normalized to the  $K$  band as in Figure 1. *Top panel:* mean SEDs in units of magnitude  $\text{arcsec}^{-2}$ . *Bottom panel:* mean SEDs in units of  $\text{mJy arcsec}^{-2}$ .

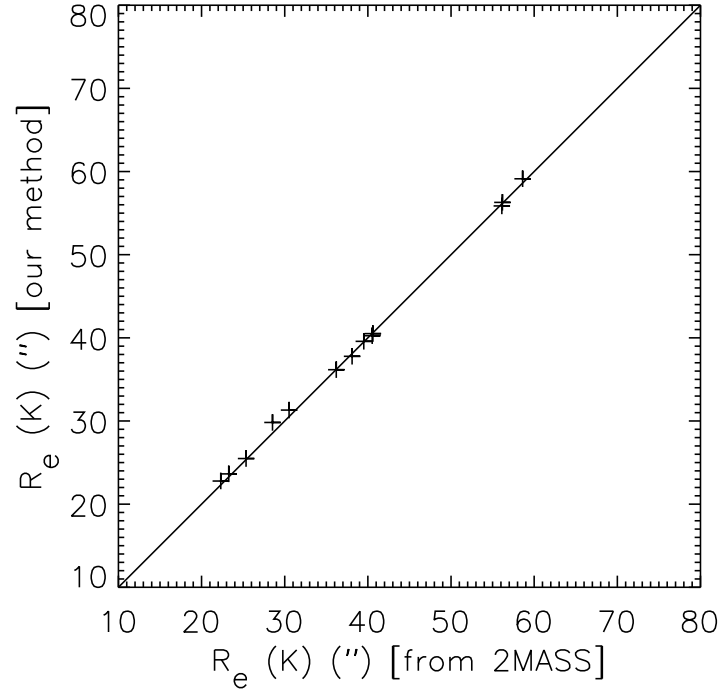


FIG. 3.— Comparison of the  $K$  band effective radius of sample galaxies measured directly from 2MASS images using our photometric procedure with  $R_e(K)$  found by Jarrett (2003) using the 2MASS procedure.

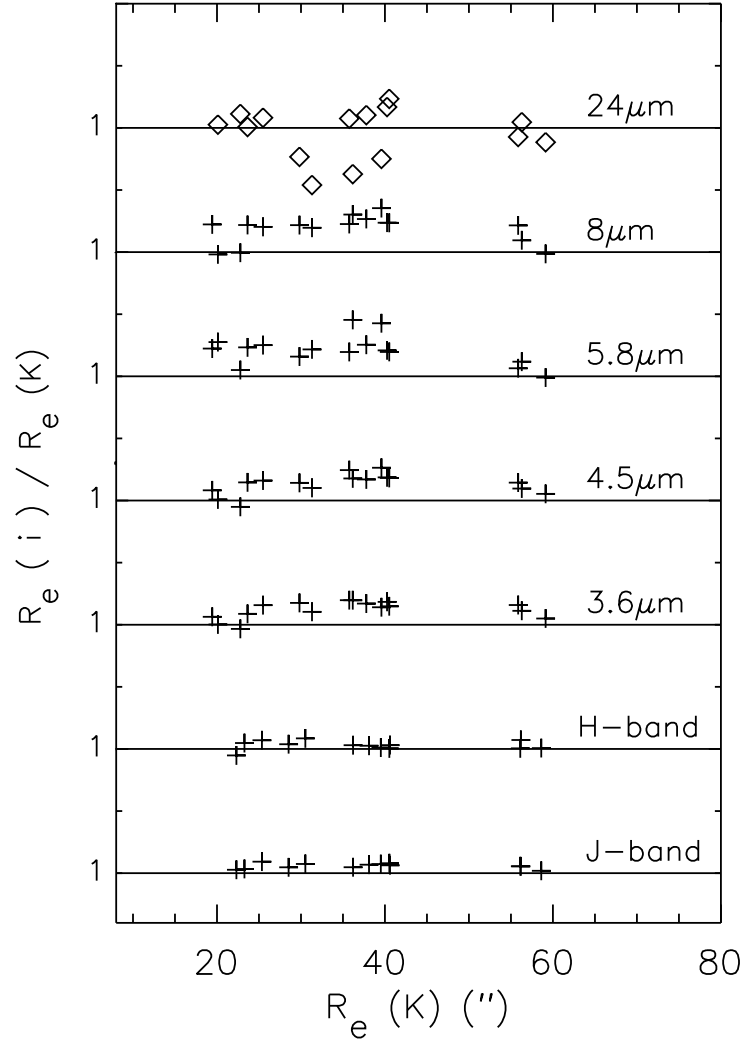


FIG. 4.— Ratios of the effective radius at seven passbands  $R_e(i)$  to the  $K$  band effective radius.  $R_e(24)/R_e(K)$  ratios are shown with open diamonds.

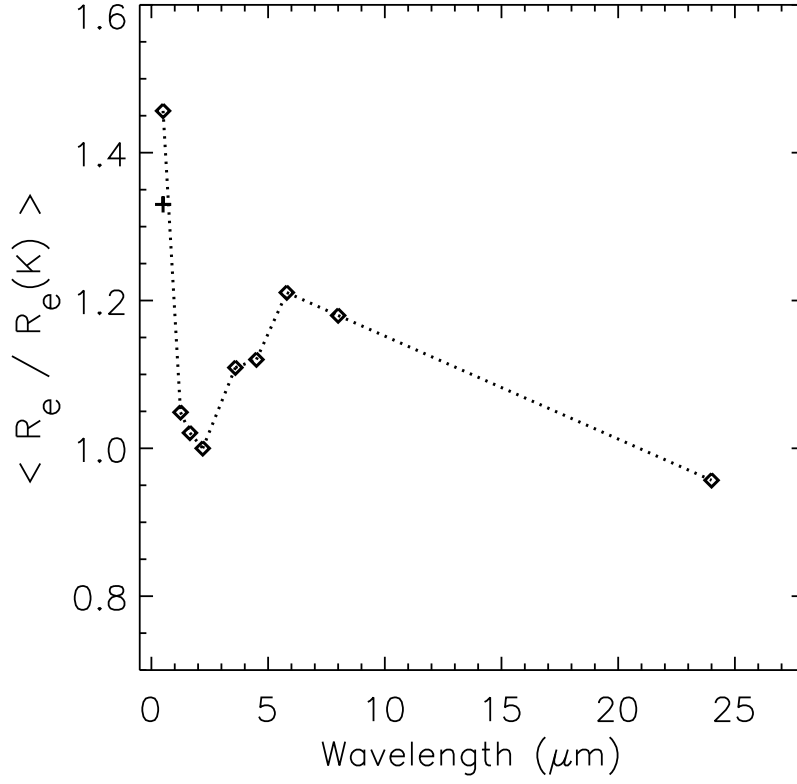


FIG. 5.— Variation with mean passband wavelength of sample-averaged ratios of the effective radii in each passband to that in the  $K$  band. Minima occur at the  $K$  band ( $2.15\mu\text{m}$ ) and at  $24\mu\text{m}$ . The + symbol shows the ratio  $\langle R_e(V)/R_e(K) \rangle$ , for 273 early type galaxies (Ko & Im 2005).

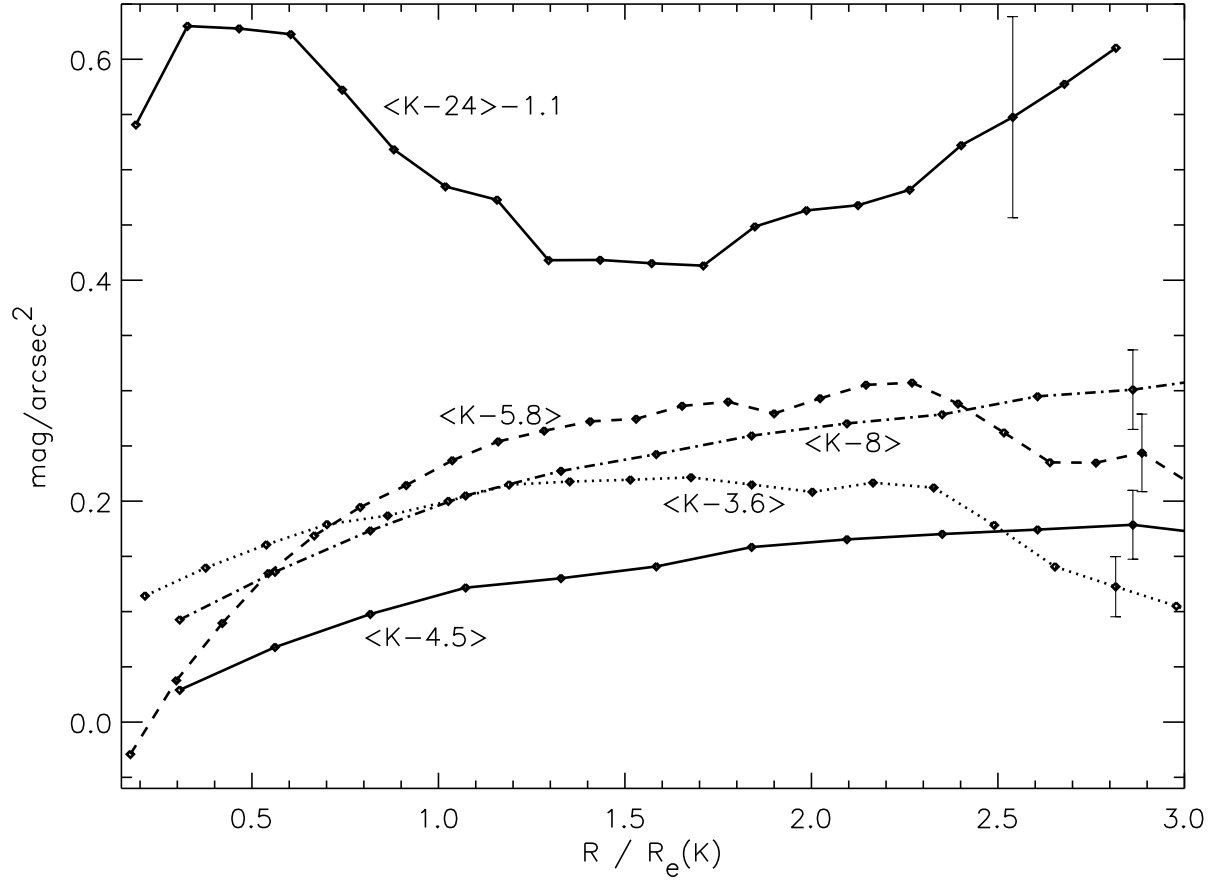


FIG. 6.— Variation of five sample-averaged radial color profiles (in surface brightness units) with galaxy radius normalized with  $R_e(K)$ .

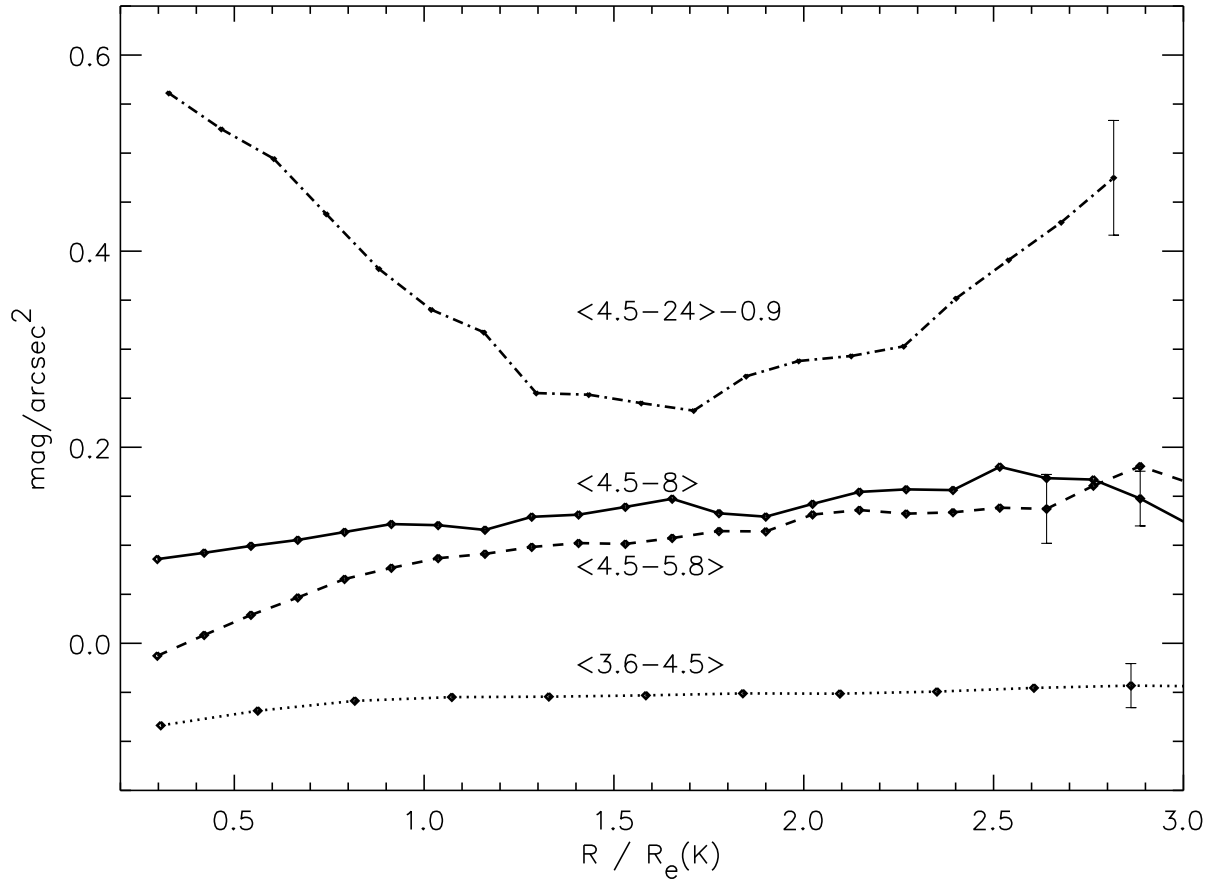


FIG. 7.— Variation of four additional sample-averaged radial color profiles (in surface brightness units) with galaxy radius normalized with  $R_e(K)$ .

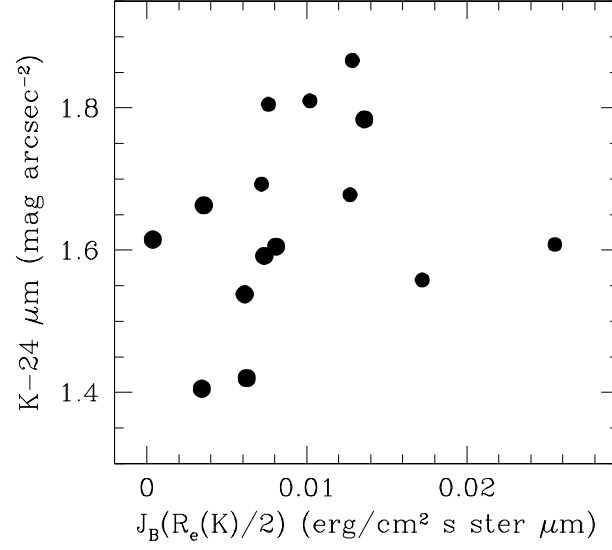


FIG. 8.— Plot showing the  $(K - 24\mu\text{m})$  color evaluated at  $R_e(K)/2$  with the mean intensity of  $B$  band diffuse galactic light at the same radius. The two outlying galaxies at the right are NGC 3379 ( $J_B = 0.017$ ) and NGC 584 ( $J_B = 0.0255$ ).

## APPENDIX

## SPATIAL RESOLUTION OF 2MASS AND IRAC PASSBANDS

In our determination of half light radii and color profiles for elliptical galaxies we have not deconvolved the surface brightness images to correct for the point spread function (PSF). In this Appendix we justify this procedure by showing that the widths of the PSFs are small compared to the K-band effective radius which characterizes the scale of the metallicity gradients of our sample galaxies.

Figure 1A shows the azimuthally averaged PSF for the 2MASS  $K_s$  and IRAC bands, all normalized to unity at the center. The FWHM of all IRAC bands are less than  $2''$  and the FWHM of the  $K_s$  band is about  $2.5''$ , only slightly larger. These PSFs are all much less than the half light radii of our sample galaxies listed in Table 2,  $R_e(K) \approx 20 - 55''$ . The PSFs alter the infrared surface brightness distributions only in the central few arcseconds which we do not discuss in this paper. Our implicit assumption that the redistribution of scattered light does not vary across the IRAC fields of view is supported by a recent study of the surface brightness of the elliptical galaxy NGC 5044 when the galactic center is placed in various non-central locations in the field of view.<sup>5</sup>

The IRAC website<sup>6</sup> at the *Spitzer Science Center* describes in some detail how to determine the surface brightness of extended objects such as elliptical galaxies and the various difficulties that can arise. An upper limit on the effect of scattered light on surface brightness color variations can be estimated, as suggested at this website, by using a double PSF convolution. Our (properly calibrated) surface brightness data  $\mu(i)$  for each passband is convolved with the PSF( $i$ ) for that passband. To evaluate the (maximum) influence of scattered light on the color  $\mu(i) - \mu(j)$ , we convolve  $\mu(i)$  with PSF( $j$ ) and  $\mu(j)$  with PSF( $i$ ), i.e. a double convolution.

The solid lines in Figure 2A show the binned surface brightness color profiles ( $K - 5.8\mu\text{m}$ ) and ( $4.5 - 5.8\mu\text{m}$ ) for elliptical galaxy NGC 6703 in which each passband is slightly broadened by the PSF of that band. These profiles are similar to the surface brightness color profiles discussed in Figures 6 and 7, except in this example they refer to a single typical galaxy, NGC 6703, not the sample average. The dashed lines in Figure 2A show the doubly convoluted color profiles in which the image in each passband is degraded by the PSF of both bands. It is clear that the radial color variations are essentially unchanged by the double PSF convolution except at  $R/R_e(K) \lesssim 0.2$  which we do not consider in our discussion. We conclude that our half light radii and radial color profiles are essentially unaffected by the 2MASS or IRAC PSFs.

At the MIPS  $24\mu\text{m}$  wavelength the PSF is somewhat larger, about  $5''$  FWHM. Nevertheless, we assume that this broadening also has little influence on the half light radius or color profiles involving the  $24\mu\text{m}$  passband, both of which vary on larger scales comparable to  $R_e$ .

<sup>5</sup> <http://spider.ipac.caltech.edu/staff/jarrett/irac/calibration/droop/>

<sup>6</sup> <http://ssc.spitzer.caltech.edu/irac/calib/extcal/>

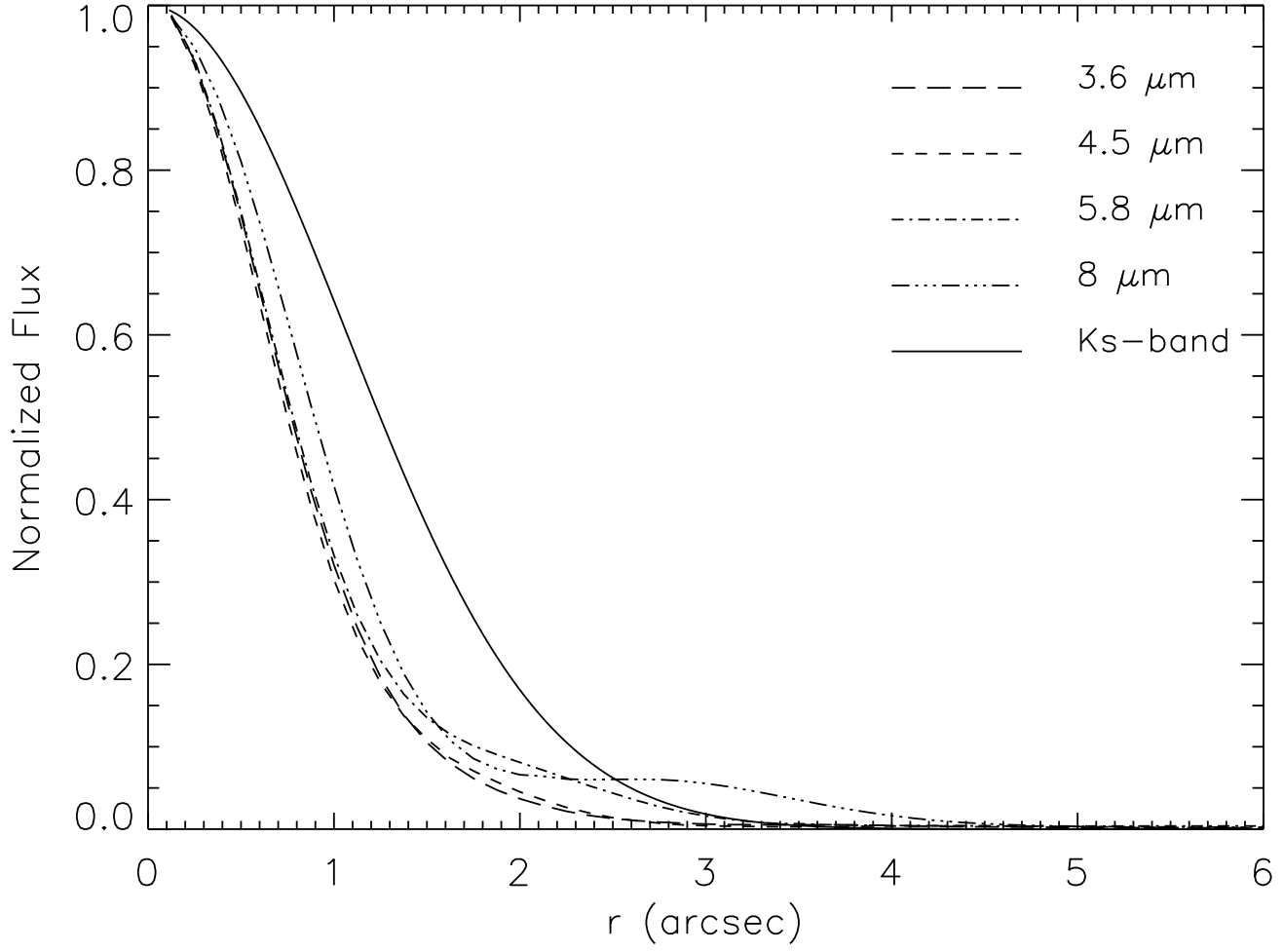


FIG. 9.— Azimuthally averaged point spread functions for the  $K_s$ -band and the four IRAC bands.

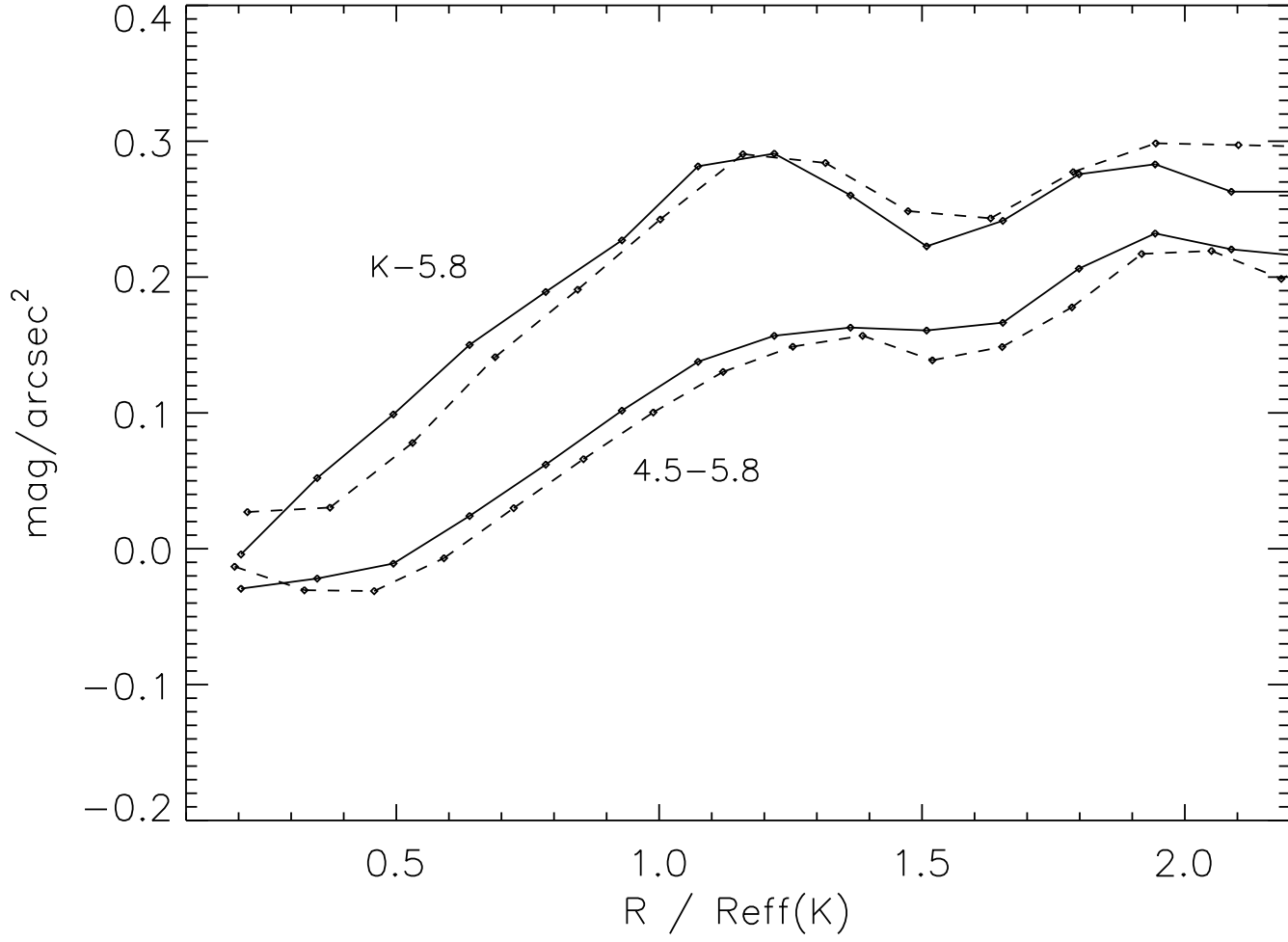


FIG. 10.— Color profiles for the galaxy NGC 6703 for singly convolved (solid lines) and doubly convolved (dashed lines) point spread functions.